

# Enthalpy–Entropy Tuning in the Adsorption of Nucleobases at the Au(111) Surface

Marta Rosa,<sup>†,‡</sup> Stefano Corni,<sup>†</sup> and Rosa Di Felice<sup>\*,†,§</sup>

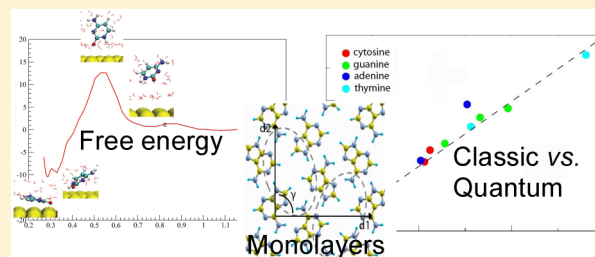
<sup>†</sup>Center S3, CNR Institute of Nanoscience, Via Campi 213/A, 41125 Modena, Italy

<sup>‡</sup>Department of Physics, University of Modena and Reggio Emilia, 41125 Modena, Italy

<sup>§</sup>Department of Physics and Astronomy, University of Southern California, Los Angeles, California 90089, United States

## S Supporting Information

**ABSTRACT:** The interaction of DNA molecules with hard substrates is of paramount importance both for the study of DNA itself and for the variety of possible technological applications. Interaction with inorganic surfaces strongly modifies the helical shape of DNA. Hence, an accurate understanding of DNA structure and function at interfaces is a fundamental question with enormous impact in science and society. This work sets the fundamentals for the simulation of entire DNA oligomers on gold surfaces in dry and wet conditions. Thanks to the new GoldDNA-AMBER force field, which was derived from first principles and includes dispersion interactions and polarization effects, we simulated self-assembled guanine and adenine monolayers on Au(111) in vacuo and the adsorption of all nucleobases on the same substrate in aqueous conditions. The periodic monolayers obtained from classical simulations match very well those from first principle calculations and experiments, assessing the robustness of the force field and motivating the application to more complex systems for which quantum calculations are not affordable and experiments are elusive. The energetics of nucleobases on Au(111) in solution reveal fundamental physicochemical effects: we find that the adsorption paradigm shifts from purely enthalpic to dominantly entropic by changing the environment and aggregation phase.



## 1. INTRODUCTION

Research on DNA has nowadays trespassed the boundaries of biological and medical laboratories and is becoming increasingly interdisciplinary, covering chemical sciences, physical sciences, and engineering/nanotechnologies. In this process, the interaction of nucleic acids with hard inorganic surfaces has assumed a primary importance.

Even within the context of life sciences, one can think of applications that require the formation of interfaces between DNA/RNA and inorganic materials: for instance, array-based sensors for DNA sequencing consist of single-stranded oligonucleotides of different sequences attached to a surface through anchoring functional groups.<sup>1</sup> The principle of operation is the complementarity of such single-stranded monolayers with the target sequences. In this kind of devices, the double helix does not contact the host substrate directly but through a linker chain that is responsible for the attachment. A similar configuration, with DNA molecules “standing” on the surface or between electrodes and attached through thiol linkers, has been successfully adopted to measure charge currents through DNA.<sup>2–6</sup>

An alternative configuration relevant in nanotechnologies embodies DNA molecules “lying” on the surface so that the backbone or bases directly contact the substrate. This is relevant for a novel vision of DNA sequencing based on physical measurements, namely translocation through nano-

pores.<sup>7,8</sup> It is mainly related to measurements of the morphology and of the electronic structure through scanning microscopes, as well as to electrical transport measurements of molecules deposited onto substrates.<sup>9–11</sup> The electrical characterization of DNA molecules is instrumental to the development of DNA-based molecular electronics and is still controversial.<sup>12–15</sup>

Modifications of the helix motif when a DNA molecule comes into contact with a hard substrate can be particularly severe. As an example of such a dramatic deviation, we refer to the results of atomic force microscope (AFM) experiments on double-stranded DNA molecules “lying” on a hard substrate: in this condition, the measured height of a DNA molecule is about 50% of the diameter of the double helix in solution.<sup>11,16</sup> This finding suggests the possible occurrence of partial unfolding, which would have strong consequences on the electrical performance. In fact, it is becoming steadily clear that the ground-state and excited-state electronic structure and the charge transfer rates in nucleobase stacks depend in a very sensitive way on the details of the atomic spatial arrangement.<sup>17–22</sup>

This brief overview introduces the concept that the knowledge and control of DNA structure–function properties

Received: December 31, 2013

Published: February 24, 2014

and their dependence on the environment (e.g., substrate versus solution) are fundamental for understanding some intrinsic features of nucleic acids that impact applications in different research fields. Experimental structural resolution of DNA molecules at interfaces is unfeasible, because conventional techniques for structure determination are specific for biological molecules or inorganic crystals. Molecular simulations thus become a powerful tool for bypassing the lack of atomic details. Classical molecular dynamics (MD) atomistic simulations are in principle the method of choice. They have successfully been employed to describe the unfolding of biological molecules in solution.<sup>23–26</sup> However, the development of force fields (FFs) suitable for the description of the adsorption of (bio)molecules at surfaces is still immature and studies of DNA/inorganic interfaces are consequently hindered. Lee and Schatz were able to perform simulations of DNA oligomers attached to metal nanoparticles,<sup>27</sup> tackling a “standing” configuration with a linker that mediates the DNA-surface connection: the presence of a linker substantially neutralizes the problem of defining a FF that encompasses the DNA–gold interaction. In order to enable simulations of “lying” configurations of DNA oligomers on a substrate, FF parameters that account for this interaction cannot be ignored. In the following, we present insights from simulations of nucleobases on a gold surface in different aggregation states and different environments, with an effective FF that has been originally developed for studying peptide adsorption on Au(111) and now tailored to study DNA adsorption on Au(111). The positive benchmark of classical simulations against quantum calculations and experimental studies is a convincing assessment of this methodology and launches the ability to predict folding motifs of double-stranded DNA oligomers on the gold surface.

The target systems of our investigation are adenine and guanine full periodic monolayers on Au(111) in vacuo and single bases on Au(111) in water solution. The choice of the substrate is dictated by our past experience on protein–Au force field generation<sup>28–30</sup> and by the existence of clear-cut experimental studies.<sup>31,32</sup> The results on the monolayers comply with experimental knowledge, proving that the classical model is robust beyond the specifically parametrized systems for which it was developed and can therefore be confidently used to simulate a variety of DNA structures on the same surface. Furthermore, they allow us to understand the limits of the Redhead approximation,<sup>33</sup> which is widely adopted for extracting values of desorption energy from the desorption rates measured in temperature programmed desorption (TPD) experiments. Encouraged by this success for the portability of the force field, we sampled a more complex environment condition that includes bulk water. We find that the environment has dramatic effects on the adsorption thermodynamics: indeed, while the monolayer formation on the substrate in vacuo is driven by enthalpy, the adsorption of individual bases (e.g., a dilute coverage regime) in solution is driven by entropy. These findings stimulate a wider exploration of aggregation states of DNA on Au(111) in diverse ambient conditions, though further tuning may become necessary when tackling such a more complex system. The entropic principle may have dramatic effects on the deposition of DNA oligomers on gold from solution drops and its understanding will eventually open the way to control sample preparation conditions in order to minimize the disruption of the helical folding motif.

## 2. METHOD

**2.1. Classical Model.** **2.1.1. Survey of Bioinorganic Force Field Development.** To the best of our knowledge, four different approaches are amenable for involvement in order to enable simulations of DNA oligomers on gold. CHARMM-METAL<sup>34</sup> was parametrized to reproduce bulk metal density and surface tension; it is compatible with CVFF<sup>35</sup> and a number of other biomolecular FFs. GOLF<sup>28–30</sup> was specifically developed for describing the interaction of proteins with the Au(111) surface with inclusion of image charge effects; it is compatible with OPLS<sup>36</sup> and CHARMM.<sup>37</sup> Zerbetto and co-workers<sup>38,39</sup> developed a FF for the adsorption on the Au(111) surface of a variety of molecules, including DNA bases. Piana and Bilic<sup>40</sup> developed special Lennard-Jones (LJ) parameters for the adsorption of DNA on Au(111), based on results of post-Hartree–Fock Møller–Plesset perturbation theory (MP2) calculations.

The CHARMM-METAL FF has been used to study the adsorption of peptides on Au(111) surfaces<sup>41–45</sup> and can in principle be used also for DNA on Au(111). Yet, we believe that it is not ideal for the description of DNA adsorption on a metal surface because of two negative built-in features. First, it neglects the dynamic polarization of the metal atoms in the Au surface. This shortcoming was presented as a source of uncertainty for the adsorption of peptides on surfaces, although its contribution was supposed to be small.<sup>45</sup> In the case of DNA, the backbone carries a  $1e^-$  charge for each nucleotide and therefore the polarizability of the substrate is not a negligible effect. Second, CHARMM-METAL was not specifically parametrized to capture individual atom–gold interactions, and consequently, it does not include terms to account for the weak chemisorption of some specific atomic species. This problem was identified in the study of peptide adsorption<sup>30</sup> and becomes dominant in the case of DNA adsorption. In fact, density functional theory (DFT) calculations with the inclusion of van der Waals (vdW) interactions pointed out that guanine, cytosine, adenine, and thymine are weakly chemisorbed on Au(111) via O and N atoms.<sup>46,47</sup>

The FF developed by Zerbetto and co-workers<sup>38</sup> is customized for the adsorption of DNA bases on Au(111). Metal polarization effects are taken into account through a charge-equilibration model that modifies the charge on the atoms during the simulation.<sup>48</sup> Moreover, long-range and weak chemisorption effects are taken into account through the fitting of interaction parameters with experimental results on nucleobase monolayers in vacuo. The main disadvantage of this approach is the computational burden: as a matter of fact, such a detailed FF is affordable only for very short simulation times for a system as complex as a DNA oligomer on the surface, and it is prohibitive to investigate a water solution environment.

Piana and Bilic were able to develop a FF that includes the vdW interaction between the bases and gold in an indirect way.<sup>40</sup> Namely, they obtained FF parameters for individual atoms from MP2 calculations of small molecules adsorbed on a planar four-atom gold cluster and then transferred them to nucleobase atoms. This approach, which was restricted by the computational cost of MP2 calculations, has the limitation of not including the specificity of the bases for what concerns adsorption on gold surfaces. Moreover, the model for the surface does not take into account polarization effects. Polarization effects can be negligible for systems such as self-

assembled base monolayers, which do not include the charged backbone but are certainly relevant for the adsorption of realistic oligomers, which is our general target.

Finally, GolP accounts for polarization of the metal atoms and can be parametrized for all the specific interactions found in DNA bases, as it was previously done for peptides.<sup>28–30</sup> GolP exists in two versions: the original GolP is compatible with OPLS<sup>29</sup> and the later GolP-CHARMM is compatible with CHARMM.<sup>30</sup> For this work, we decided to use a GolP-like FF that is designed for nucleic acids rather than proteins and is compatible with AMBER, which is acknowledged as the most reliable classical description of DNA in solution:<sup>49–54</sup> we will call the new FF GoldDNA-AMBER. Some authors have addressed the problem if FF parameters derived for biomolecules in solution are directly transferable to biointerfacial simulations.<sup>55,56</sup> This question is still unanswered. Yet, at present, a FF for gold–DNA interaction that is consistent with an existing bio-organic FF, such as AMBER, is the only viable way to predict adsorption equilibria from computational simulations. At the present stage, it is known that the procedure to generate classical force field parameters from DFT is consistent, though the resulting parameters are not necessarily universal and should be evaluated through extensive applications.<sup>57–60</sup>

**2.1.2. GoldDNA-AMBER.** In GoldDNA-AMBER the potential energy function for the interaction between DNA bases and the Au(111) surface is written as<sup>29</sup>

$$V_{\text{Au-DNA}}^{\text{tot}} = V_{\text{Au-DNA}}^{\text{im}} + V_{\text{Au-DNA}}^{\text{vdW}} + V_{\text{Au-DNA}}^{\text{bonding}} \quad (1)$$

$V_{\text{Au-DNA}}^{\text{vdW}}$  and  $V_{\text{Au-DNA}}^{\text{bonding}}$  are the van der Waals and bonding interaction terms between atoms in the DNA base and gold atoms.  $V_{\text{Au-DNA}}^{\text{im}}$  is the Coulombic electrostatic interaction between the molecule and the image charges induced in gold.

The surface polarization effect is described through a dipole located in the position of each gold atom. One such dipole is constituted of two opposite charges, connected by a rigid rod free to rotate around one end.<sup>28</sup> In the absence of a molecule on the surface, the average dipole moment is equal to zero, with the initial orientation of the dipoles chosen randomly. When a molecule lies above the surface, the partial atomic charge on its atoms forces the rods to preferentially rotate in a specific orientation, modifying the average dipole moment. This model is computationally efficient<sup>29,61,62</sup> and able to reproduce continuous electrostatics results.<sup>28</sup> It was demonstrated for GolP<sup>28,29</sup> and GolP-CHARMM<sup>30</sup> that including polarization effects facilitates the transferability of parameters derived in the gas phase to the condensed phase (e.g., this was demonstrated for the AMOEBA FF<sup>63</sup> that is specific for biomolecules). This means that parameters fitted to in vacuo reference data are suitable for the study of molecules adsorbed on gold in solution. GoldDNA-AMBER gold atoms are held frozen during the simulation, therefore it is not necessary to define an interaction between them. This means that this FF is not useful for describing the gold surface itself but is focused on the adsorption of molecules on it. The Au(111)  $22 \times \sqrt{3}$  surface reconstruction, in particular, has not been taken into account, as only marginally small differences exist between the reconstructed and ideal surfaces,<sup>64</sup> which are negligible for the purposes of this work. Moreover, an optimization of interaction parameters of water molecules allows GoldDNA-AMBER to describe DNA adsorption not only in vacuo but also in aqueous conditions.<sup>30</sup> The parametrization of GoldDNA-

AMBER relies on a multistep approach based on DFT results. Details are reported in the Supporting Information.

Bonding and vdW interactions are together described through a sum of 12-6 Lennard-Jones interactions (eq 2) between each DNA atom and interaction sites on the gold surface:

$$V^{\text{vdW}}(r_{ij}) = 4\epsilon_{ij} \left[ \left( \frac{\sigma_{ij}}{r_{ij}} \right)^{12} - \left( \frac{\sigma_{ij}}{r_{ij}} \right)^6 \right] \quad (2)$$

In GoldDNA-AMBER, as in GolP and GolP-CHARMM, the topmost layer of the surface slab includes real gold atoms and virtual interaction sites. Virtual sites are placed in hollow positions of the real lattice and are the ones interacting with adsorbing species via the LJ terms, while the LJ parameters of real gold atoms are set to zero. Dipolar rods are located only on gold atoms. This formulation allowed us to achieve the correct description of the adsorption of small molecules at top sites rather than at hollow sites.<sup>29,30,65</sup> This is important for this study, because also DNA bases prefer top adsorption sites,<sup>47</sup> although they are characterized by a pronounced lateral mobility.<sup>38</sup> Our results reported later satisfy both these conditions, which we have posed as a requirement for the positive evaluation of our classical model.

If no particular interaction is defined, LJ parameters for gold atoms ( $\sigma_{\text{Au}}$ ,  $\epsilon_{\text{Au}}$ ) are combined with LJ parameters for DNA atoms, in accordance with AMBER Lorentz–Berthelot mixing rules,  $\sigma_{ij} = (\sigma_i + \sigma_j)/2$ ,  $\epsilon_{ij} = (\epsilon_i \epsilon_j)^{1/2}$ . Ad-hoc LJ parameters can be defined for the interaction between some atoms and the Au surface. Such adjusted LJ interactions account for dispersion, repulsion and weak chemisorption effects. Details of our choice of GoldDNA-AMBER parameters, along with the tuning procedure, are given in the Supporting Information.

## 2.2. Computational Approach. 2.2.1. DFT Calculations.

We performed plane-wave pseudopotential DFT calculations with the quantum-espresso package version 5.0,<sup>66</sup> using the vdW-DF functional.<sup>67</sup> This choice of the functional was a consequence of several tests to assess the performance of similar functionals,<sup>67–72</sup> on model interfaces, benzene@Au(111), ammonia@Au(111), cytosine@Au(111), which will be addressed in a dedicated publication.<sup>73</sup>

The two adenine and guanine self-assembled monolayers, which we label  $A_{\text{IML}}@Au(111)$  and  $G_{\text{IML}}@Au(111)$ , respectively, were simulated in the repeated supercell approach: the size of the supercells was chosen according to periodicities revealed in experimental data but was optimized by DFT. Each supercell contained a single nucleobase layer at full coverage (4 guanines, 12 adenines) and a gold slab with four layers. We adopted a kinetic energy cutoff of 25 Ry for the plane-wave expansion of the wave functions (200 Ry for the charge density),<sup>65</sup> and we described the electron-ion interaction with ultrasoft pseudopotentials.<sup>74</sup> Brillouin zone sums were calculated including two Monkhorst–Pack special  $k$  points in the irreducible wedge. In calculations for structural optimization all the atomic coordinates were relaxed until each force component vanished within 0.05 eV/Å.

The lateral size of the supercells (parameters  $d1$ ,  $d2$ , and  $\gamma$ , Figure 1) for guanine and adenine self-assembled monolayers on Au(111) was fixed to respect the periodicity of the overlayers observed in experimental studies (Figure 1), while being a multiple of the triangular lattice of the gold substrate. The triangular lattice constant of Au(111) was set to 3.0 Å,<sup>46</sup>



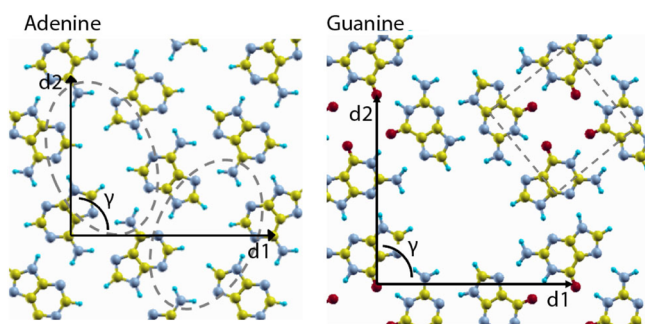


**Figure 1.** Periodicity of adenine<sup>31</sup> and guanine<sup>32</sup> monolayers as reported from scanning tunneling microscope measurements.  $d_1$ ,  $d_2$ , and  $\gamma$  are the unitary cell parameters. The gray dashed line in each panel marks the repeating unit of the monolayer.

which is the equilibrium value computed by DFT with the vdW-DF functional, consistently with the monolayer calculations. This value expresses an overestimation by about 4% of the experimental value. The Supporting Information reports additional details on the supercells and on the evaluation of the formation energy.

**2.2.2. Classical MD Calculations.** All the FF-based simulations were performed with the Gromacs 4 MD simulation package<sup>75</sup> in the NVT ensemble using a Nosé–Hoover thermostat. The Particle Mesh Ewald (PME)<sup>76</sup> electrostatic summation was used with a real-space cutoff at 11 Å. A force-switched cutoff starting at 9 Å and ending at 10 Å was used for Lennard-Jones nonbonded interactions. The amber99sb<sup>54</sup> version of the AMBER FF was applied to the nucleic acids and the GoDNA-AMBER FF was applied to the substrate coupled to the bases. Each MD simulation was preceded by a standard minimization-equilibration protocol. Details are given in the Supporting Information (supercells, formation energies, and free energies).

### 3. RESULTS AND DISCUSSION

**3.1. Self-assembled Guanine and Adenine Monolayers on Au(111).** DNA bases self-assemble in periodic overlayers on the Au(111) surface, with a two-dimensional periodicity for guanine and adenine. The structure of such bioinorganic interfaces has been intensively studied by scanning tunneling microscope (STM) measurements in combination with DFT calculations.<sup>31,32,77–80</sup> These investigations convey a description of the structure of guanine and adenine monolayers on Au(111), which was a precious precondition for our investigation, avoiding the need for sampling many different supercell sizes. Data on desorption energies for base monolayers on Au(111) also exist, from TPD infrared reflection absorption spectroscopy (TPD-IRAS) and TPD mass spectroscopy (TPD-MS) experiments.<sup>81</sup> By calculating formation energies for the computed monolayer structures that map the STM images, we are in place to benchmark QM and MM results against experimental data of desorption energies, for validation of the GoDNA-AMBER FF and its use for prediction of the behavior of nucleobases on the surface immersed in a water solution. We find, indeed, that the force field is robust and transferable to systems different from those used for the parametrization. We discuss the results of DFT calculations, the performance of FF simulations and finally the approximations that are implicit in comparing our formation energies to experimental desorption energies, which are not

measured directly but are indirectly estimated from measured quantities.

Besenbacher and co-workers<sup>31,32</sup> predicted the atomic structures of guanine and adenine self-assembled monolayers on Au(111) by combining STM images and DFT results not accounting for vdW terms in the functional. They generated several regular monolayer structures, characterized by different possible patterns of hydrogen bonds. They carried out DFT calculations of a number of unsupported monolayers that best fit the STM images, optimizing the lateral size (Figure 1). They eventually ranked the computed structures in energy and found a fair agreement of the size of the lowest-energy structures relative to the experimental measurements. All the DFT calculations were done on gas-phase structures, not adsorbed on the surface, under the assumption that the base–gold interaction is negligible.

We actually showed that the base–gold coupling is not negligible and goes beyond pure dispersion interactions; in fact, we even found electronic hybridization.<sup>46,47</sup> It is therefore important to correctly describe the presence of the substrate in order to attain a quantitative description of the adsorption energies and structures. We discussed in our recent work the importance of using a functional that is able to estimate van der Waals effects in DFT calculations of single nucleobases on Au(111) in vacuo and we start our analysis by monitoring the importance of these effects in the self-assembled monolayers, by assessing vdW-DF results against PBE results.

We evaluated the length of covalent bonds and of H-bonds for adenine gas-phase dimers ( $A_2$ ) with the vdW-DF and PBE functionals and for the same dimers adsorbed on Au with the vdW-DF functional. Results show that the bonding lengths are equivalent in the three cases. This evidence is an indication that van der Waals effects and the presence of the surface are not strong factors in determining the inherent geometry of the monolayers. This is an interesting outcome of our calculations: while we know that vdW effects are conspicuous on the binding energies,<sup>46,47</sup> they are weak on the adsorbate atomic structures. The negligible effect of the surface is in line with the large lateral mobility of single DNA bases adsorbed horizontally on Au(111) emerging from our DFT calculations (quasi-degeneracy of various adsorption sites within 1.5 kcal/mol).

We then checked the possible role of the vdW treatment in the energetic ranking of different unsupported adenine monolayers that were found compatible with STM data.<sup>31</sup> Specifically, we evaluated with the vdW-DF functional the relative energy for the three most favorable geometries identified in agreement with morphological measurements, following the procedure previously suggested.<sup>31</sup> In these vdW-DF calculations, the structure was not relaxed and the supercell size was fixed according to the published work<sup>31,32</sup> (see Supporting Information for details). We found the same global minimum as that identified without the vdW treatment (Table S5 in Supporting Information). We further checked the accuracy of the lateral size of the periodic monolayer unit. To this aim, we performed a series of self-consistent calculations for the unsupported monolayers at variable supercell size, by changing the parameters  $d_1$ ,  $d_2$ , and  $\gamma$ . The computed equilibrium supercell parameters are still in agreement with STM measurements and the energetic order is still in agreement with the published DFT results (see Supporting Information). These tests, performed by us at a higher level of theory, validate the structure and energetics obtained with the simpler approach: consequently, we concluded that the

inherent geometries of the guanine and adenine monolayers proposed by Besenbacher and co-workers are faithful for use in the following calculations for the surface-supported monolayers. The same procedure was followed for calculating the equilibrium values of  $d1$ ,  $d2$ , and  $\gamma$  for the guanine unsupported monolayer (Table S6 in Supporting Information). The adjustment to comply with the substrate lattice registry and size, as well as the supercells for FF calculations, are described in the Method section.

The formation energies of the adsorbed monolayers obtained from our vdW-DF and FF calculations are reported in Table 1.

**Table 1.** Calculated Formation Energies by DFT and MM +MD and Measured Desorption Energies, in kcal/mol

system		computed $E_{\text{form}}^a$		measured $E_{\text{des}}^d$
		DFT <sup>b</sup>	FF <sup>c</sup>	
adsorbed full monolayers in vacuo	$A_{\text{IML}}@Au(111)$	−34.6	−34.8	$29.6 \pm 0.7$
	$G_{\text{IML}}@Au(111)$	−41.2	−42.8	$30.5 \pm 0.5$
adsorbed partial monolayers in vacuo	$G_{(1/6)\text{ML}}@Au(111)$		−31.3	
adsorbed bases in water solution	$A@Au(111)_{\text{H}_2\text{O}}$		$1.4 \pm 0.4$	
	$G@Au(111)_{\text{H}_2\text{O}}$		$0.6 \pm 0.4$	
	$T@Au(111)_{\text{H}_2\text{O}}$		$3.0 \pm 0.8$	
	$C@Au(111)_{\text{H}_2\text{O}}$		$1.2 \pm 0.4$	

<sup>a</sup>The negative values of the formation energy indicate favorable adsorption reactions. <sup>b</sup>The DFT formation energy is evaluated by eq 1 in the Supporting Information. <sup>c</sup>The FF formation energy is evaluated as the sum of formation energies from the LJ, Coulomb, and bonding terms. (See Supporting Information: Sum of eqs 2 and 3 for the monolayers in vacuo and sum of eqs 4 and 5 for the single bases in water). <sup>d</sup>The measured desorption energy is taken from published work.<sup>81</sup> The positive values of the desorption energy indicate that desorption is an unfavorable process and must be activated.

This is a pristine result of this work: The DFT values could not be evaluated earlier by considering only the unsupported monolayers; the classical calculations were missing a proper FF for the monolayer-substrate interactions. Table 1 also compiles the formation energies of interfaces between single bases and Au(111) in water, which are elaborated in the next section.

Before commenting on the accuracy of FF simulations, we include the analysis of the electronic structure from DFT, which is another original ingredient of this article. Electronic hybridization and bonding orbitals were detected at the interfaces between individual bases and Au(111) in vacuo: it is a fundamental question to unravel whether this property extends to the larger scale of periodic monolayers.

In Figure 2 we illustrate the electronic density of states (DOS) of the  $G_{\text{IML}}@Au(111)$  system, compared to that of the  $hG'@Au(111)$  interface (namely, a single guanine adsorbed on Au(111) in vacuo in a horizontal configuration with the O atom on top of a Au atom) from our previous study.<sup>47</sup> The similarity between the solid and dashed green lines testifies that the molecular electron states are similarly distributed at the two interfaces. In the HOMO energy range (−1 eV) the two curves are practically identical. Shape differences emerge in the energy

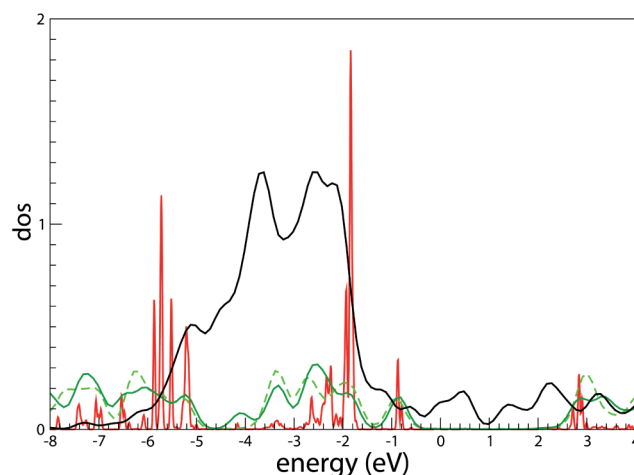


**Figure 2.** DOS of the optimized  $G_{\text{IML}}@Au(111)$  and  $hG'@Au(111)$  structures. The origin of the energy scale is set at the Fermi level of the monolayer. The deepest occupied energy level, which is associated to the same orbital in the guanine monolayer and in the isolated guanine molecule, is used for alignment of the different curves. The green solid line is the projection of the total  $G_{\text{IML}}@Au(111)$  DOS on the guanine molecules of the monolayer, normalized to one guanine. The black line is the projections of the total  $G_{\text{IML}}@Au(111)$  DOS on the outermost substrate layer. The red line is the projection of the total  $G_{\text{IML}}@Au(111)$  DOS on the O atoms of the monolayer, normalized to one O atom. The green dashed line is the projection of the total  $hG'@Au(111)$  DOS on the guanine molecule. The projected DOS curves are computed by projecting the total DOS onto atomic orbitals and then summing over all the projections that constitute the subsystems of interest.

range −1.5/−4.0 eV, where the monolayer has a more disperse guanine-projected DOS.

We note in Figure 2 energy intervals where the projected DOS on both guanine and Au is finite, which is a possible index of electronic coupling. The analysis of the electronic structure for  $hG'@Au(111)$ , as well as for the similar systems with the other bases, revealed indeed a special kind of hybridization between adsorbate and substrate. By inspecting the electronic functions in relevant energy ranges, between 0.0 eV and −4.0 eV, we find the same electronic mixing for the periodic guanine monolayer  $G_{\text{IML}}@Au(111)$  as for the nonperiodic  $G@Au(111)$  interface. The guanine HOMO forms hybrid orbitals with the substrate around −1.0 eV, with nodes in the interface region. The guanine HOMO-1 forms bonding orbitals with the substrate in the energy range −2.0/−4.0 eV: one such example is shown in Figure 3. The mechanism for this molecule–substrate pairing was extensively discussed elsewhere: it is intermediate between the Newns–Anderson chemisorption model and pure physisorption.<sup>47</sup> Similar findings apply to the

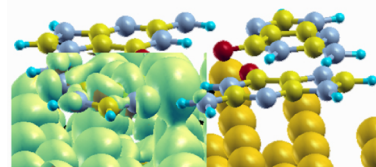


**Figure 3.** Isosurface plot of an orbital orbital of  $G_{\text{IML}}@Au(111)$  at −3.0 eV, which shows a bonding character between the adsorbate and the substrate. The molecular component of this orbital stems from the first occupied orbital below the HOMO of isolated guanine.

adenine monolayer  $A_{1ML}@Au(111)$ . The exact energies of the hybrid orbitals, as well as their components in terms of molecular orbitals, may be affected by the DFT description and GW corrections would offer more accurate electronic spectra. However, this issue should not qualitatively affect the adsorption mechanism. Note, in addition, that GW corrections known for isolated DNA bases<sup>82</sup> cannot be assumed in the interface configuration.<sup>83</sup>

The values in Table 1 show that the classical results are in good agreement with DFT results, within 1.6 kcal/mol that is the FF accuracy. We conclude that the GoDNA-AMBER force field, which parameters were obtained by fitting classical to quantum energies for interfaces of single bases with gold in vacuo, is robust beyond the specific parametrized systems. In particular, it is transferable to systems where interaction occurs not only between the adsorbate and the substrate but also within the adsorbate. Confident in this positive feedback, we use it in the next section to investigate the role of an aqueous environment in nucleobase–gold reactions, with a plethora of implications for biological problems.

Yet, let us also discuss the relation between computational results and experimental data. Both DFT and FF calculations overestimate the measured formation energies by 20–40%. This discrepancy calls for a deeper inspection: it is important to explain how the experimental desorption energy is indirectly extracted from the measurements.

TPD estimates of the desorption energy are derived from the measured desorption rate  $N(t)$  according to the Redhead formula:<sup>33</sup>

$$N(t) = \nu N_s \sigma^n \exp(-H_d/k_B T_d) \quad (3)$$

where  $\nu$  is a pre-exponential factor that depends on atomic masses and bond strength,  $N_s$  is the number of available surface sites,  $\sigma$  is the surface coverage,  $n$  is the order of the desorption reaction,  $H_d$  is the formation enthalpy,  $k_B$  is the Boltzmann constant, and  $T_d$  is the desorption temperature. The evaluation of the desorption enthalpy is usually done assuming that it is independent of surface coverage and that desorption follows a first-order kinetics ( $n = 1$  in eq 3),<sup>86</sup> using a standard value of  $\nu = 10^{13} \text{ s}^{-1}$ , assuming that the partition function for the free and adsorbed molecule are the same, apart for the degree of freedom along the dimension normal to the surface.<sup>84</sup> The latter assumption is controversial:<sup>84–87</sup> an agreement on a suitable evaluation method for a more accurate pre-exponential factor is elusive, but it is widely accepted that it should depend on the size of the adsorbate molecule. A more accurate evaluation of both  $\nu$  and  $H_d$  can be achieved by performing desorption experiments with different coverages and temperatures and fitting the results with the Polanyi–Wigner equation,<sup>85</sup> which is equivalent to the Redhead equation with a coverage-dependent  $H_d$ . For the evaluation of desorption energies of nucleobase monolayers on Au(111), the simple Redhead formula was adopted with a fixed  $\nu = 10^{13} \text{ s}^{-1}$  and a coverage-independent  $H_d$ .<sup>81</sup> We argue that this approximation introduces errors in the experimental estimates, which are partly the source of the apparent discrepancy with our calculations. During the desorption process a progressive detachment of the molecules takes place, but in the Redhead estimation of the desorption energy from the measured rate, the energy itself is considered to be independent of the coverage. This assumption yields a systematic underestimation of the effective desorption energy when adsorbate–adsorbate interactions are favorable, as in the cases studied here.

To understand whether this assumption is substantially responsible for the deviation of the computed formation energies (Table 1) from the experimental data of desorption energies, we calculated the formation energy of an interface at lower guanine coverage. We considered the single guanine unit of Figure 1, which contains the four guanine molecules marked by the dashed rectangle: we refer to this system as  $G_{(1/6)ML}@Au(111)$ , because the coverage is 1/6 relative to the full guanine monolayer (see section Method). We made this choice because experimental data indicate that the molecules first adsorb in units of four G molecules and then cover all the surface.<sup>81</sup> The formation energy per guanine, relative to gas-phase guanine molecules, is much smaller than the formation energy of the monolayer  $G_{1ML}@Au(111)$  and is a slight overestimation of the reported experimental value, by only 3%, which is a great improvement with respect to the 40% overestimation for the monolayer. The formation energy of  $-31.3 \text{ kcal/mol}$  for  $G_{(1/6)ML}@Au(111)$  is a lower limit for the desorption energy in the case of a partial coverage of the surface. We can safely state that the Redhead approximations in the evaluation of the desorption energy from TPD experiments cause an underestimation of the real value, because of the too low value that is conventionally adopted for the pre-exponential factor and of the missing dependence on the surface coverage in the right-hand side of eq 3. We do not claim a guess for the correct value of the experimental desorption energy for the monolayers, but we can estimate a similar agreement for guanine as for adenine, namely a precision within 5 kcal/mol. For what concerns the geometry, we correctly describe the structure proposed on the basis of STM imaging by both DFT and FF calculations.

**3.2. Single Bases in Water.** The FF computed values of formation energy are reported in Table 1. The errors of each component of the energy were estimated by the block averaging technique as implemented in the *g\_analyze* Gromacs utility.<sup>75,88</sup> The formation energy is positive for all four adsorbed systems; that is, the adsorbed configurations are enthalpically unfavored with respect to the solvated bases. This result differs from what we know for the adsorption of nucleobases on the same substrate in vacuo<sup>47</sup> (Supporting Information). Nevertheless, we find that once the molecule is adsorbed on the surface, it does not desorb during the whole MD simulation, indicating a preference for the adsorbed configuration.

We then performed two longer MD simulations, 100 ns at 300 K, with guanine and cytosine starting in the middle of the cell immersed in bulk water. In both cases, the molecule adsorbed on the surface after approximately 30 ns and it did not desorb during the rest of the simulation: this evidence suggests that the free energy should be representative of the adsorption energetics rather than only the enthalpic term. We speculated that the free energy of formation should be negative if the interface is formed from the solvated molecule. This implies that the entropic term, which accounts for the entropy change in adsorbing the DNA base and desorbing the corresponding water molecules from the gold and molecular surfaces, contributes sizably to the free energy of the adsorption process and favors the adsorbed configuration over the solvated one. Indeed, the adsorption energies in Table 1 are tiny, so that the entropy easily becomes determinant. To verify this picture, we computed the free energy of interaction for cytosine as an illustrative example, by means of MD potential of mean force calculations.



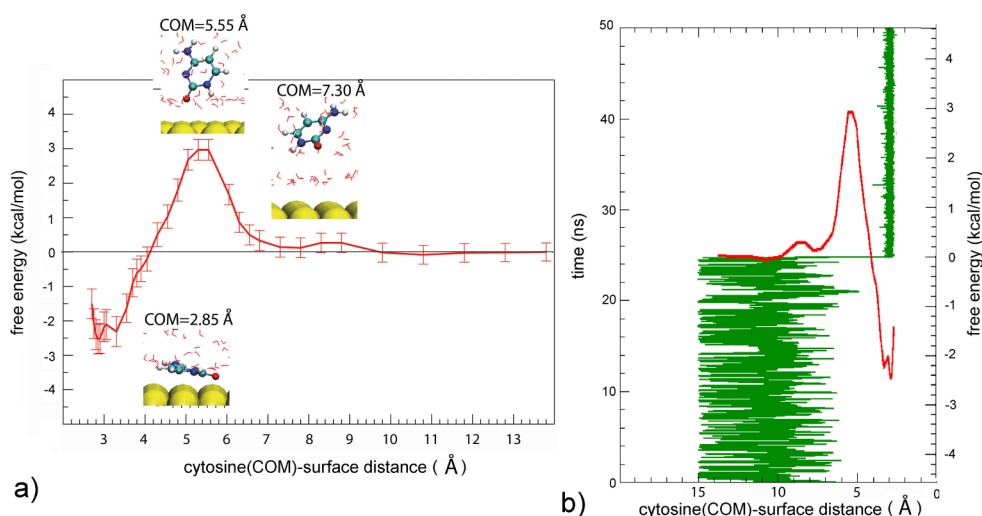


**Figure 4.** (a) Plot of the free energy landscape for  $C@Au(111)_{H_2O}$ ; insets show snapshots from restrained MD runs for the free-energy calculation. (b) Superposition of the free energy profile (red) to the cytosine(COM)–Au distance in time (green): the latter is extracted from the 100-ns free-MD trajectory and fluctuates always in the same manner after 25 ns.

The results are illustrated in Figure 4, which reports the free energy of formation of the interface between cytosine and Au(111) in a water solution, as a function of the cytosine-(COM)-surface distance. The lowest-free-energy minimum occurs when the COM of the molecule is at a distance of 2.85 Å from the surface, confirming the preference of the molecule for the adsorbed configuration. The free energy difference between the adsorbed and the solvated configuration is equal to  $-2.6 \pm 0.3$  kcal/mol. This result demonstrates that the adsorption of cytosine on Au(111) in water is determined by the entropic contribution, in contrast with the results obtained for the system in vacuo where the enthalpic contribution alone explains the  $C@Au(111)$  interface. The adsorption process can be further unraveled by analyzing the cytosine orientation with respect to the surface at different COM-surface distances. The insets in Figure 4a visualize various configurations that occur in the restrained MD runs, with the COM of the adsorbate at different distances from the substrate. At the distance of 2.85–3.05 Å two minima are present: the first one corresponds to cytosine adsorbed horizontally on the surface, slightly tilted in the same geometry found in vacuo with DFT calculations. In this case the molecule is adsorbed just above the surface, with its reactive O atom below any water molecules (see inset at 2.85 Å) and the geometry is consequently similar to the one obtained in vacuo. The second minimum is practically degenerate with the first one. It is probably due to another adsorption configuration that exists also in vacuo,<sup>47</sup> very close in energy to the most favorable configuration but with the molecular plane almost perpendicular to the surface. At a distance of 5.55 Å, there is a maximum of the free energy. The inset at 5.55 Å shows that the O2 atom of cytosine and some water molecules are at the same distance from the substrate. This geometry is strongly unfavored, as water is displaced from the gold and cytosine surfaces but the gold–cytosine interaction is not strong enough to balance the unfavorable dehydration. From DFT calculations we know that the N3–Au interaction complements the O2–Au interaction, thus fortifying the adsorption mechanism. However, at such a large distance from the surface N3 is well screened by water molecules and does not react with gold. At the distance of 7.30 Å we find a shallow local minimum, characterized by a thick

water layer between substrate and adsorbate. This analysis allowed us to better understand the balance between the enthalpic and entropic contributions in the adsorption process. The interaction of water molecules with both the nucleobase and the gold surface is strong enough with respect to the interaction between the nucleobase and the surface to favor the desorbed configuration with respect to the adsorbed one. The fundamental contribution to the adsorption process comes from entropy: the adsorption of the nucleobase on gold allows water molecules to diffuse in the solution, supplying a positive entropic contribution to the free energy. This contribution determines the final free energy profile and the system preference for the adsorbed configuration. Once the molecule is adsorbed on the surface, desorption is unfavored not only by the difference in the free energy value between the two configurations, but more notably by the presence of a free energy barrier. The barrier is due to the competition between water and cytosine for gaining the surface: the relative cytosine–Au and water–Au distances are responsible for the shape of the free energy profile.

The plot in Figure 4b superposes the free energy profile to the cytosine(COM)–gold distance as a function of time. The latter is from the free-MD trajectory of 100 ns starting with solvated cytosine, during which the maximum distance between the cytosine and the periodic image of the surface was 1.5 nm. From this plot we learn that the molecule spent some time in water before eventually overcoming the barrier and getting adsorbed on the surface, where it remained afterward for the entire duration of the MD run.

This interplay between entropy and enthalpy is further analyzed in Figure 5, which displays the densities of water molecules and of cytosine O2 atoms along the reaction coordinate  $d$ , which is the water(O)–Au and cytosine(COM)–Au distance, respectively. The blue area represents the distribution of water molecules on Au(111) from an independent free MD simulation (7.5 ns at 300 K) in the absence of cytosine, in the same  $8 \times 5\sqrt{3}$  supercell: the first and most intense peak of water density occurs at a water(O)–Au distance that coincides with the cytosine(COM)–Au distance at the lowest-free-energy minimum (Figure 4). This is an additional evidence that the cytosine and water molecules

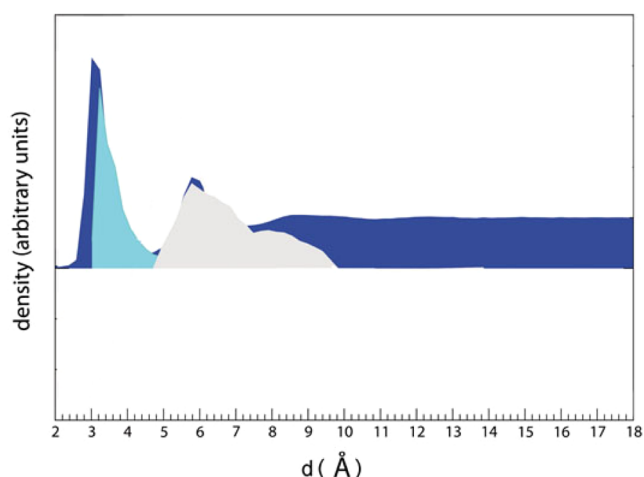


**Figure 5.** Relation between free energy profile and adsorbate densities. Blue: density of water molecules along the direction perpendicular to the surface, in the absence of any other adsorbate species. Cyan: density of cytosine O2 atoms when the cytosine COM is restrained at 5.55 Å from the surface (this cytosine location corresponds to the maximum of the free energy in Figure 4a). Gray: density of cytosine O2 atoms when the cytosine COM is restrained at 7.30 Å from the surface (this cytosine location corresponds to the shallow minimum of the free energy immediately after the barrier in Figure 4a). The reaction coordinate on the horizontal axis is the water(O)–Au distance for the blue curve, the cytosine(COM)–Au distance for the cyan and gray curves.

are competing for the surface at that distance and that the adsorbed molecule must replace a layer of interacting water molecules. The cyan area represents the O2 density during the restrained MD simulation with the cytosine(COM)–surface distance of 5.55 Å, a condition that corresponds to the free-energy barrier: therefore, as we already inferred above, the energy barrier corresponds to a situation in which the O2 atoms approach locations that are the preferred ones for water and must displace the water molecules before getting closer to the substrate. In other words, the barrier is due to the unfavored displacement of water from the interface. The gray area represents the O2 distribution during the restrained MD simulation with the cytosine(COM)–surface distance of 7.50 Å, which corresponds to the shallow local minimum of the free energy (Figure 4). In this condition the O2 peak coincides with the second water density peak and the O2 atoms maximize the interaction with water molecules.

Comparison between experimental and computational results could not be done for DNA bases adsorbed on Au(111) in aqueous conditions because of the lack of experimental data. Yet, the similarities of our results to those obtained using a similar procedure for peptides adsorbed on Au(111)<sup>30</sup> validate the approach and the outcome.

#### 4. SUMMARY

In conclusion, thanks to the derivation of the tailored GoldDNA-AMBER FF, we were able to study the adsorption of DNA bases on the Au(111) surface both in vacuo and in aqueous conditions.

Our quantum and classical results for the monolayer formation energies and geometries are unprecedented. They were obtained with a special functional for vdW effects and a tailored force field, respectively. They are in agreement with experimental data. They allow us to confirm the robustness of

the GoldDNA-AMBER force field and to rationalize the effects of varying coverage on the evaluation of desorption energy from TPD experiments.

The free energy calculations give us insights into the particular adsorption mechanism of DNA bases on Au(111) in water. We find that the interaction between nucleobases and the surface, which is the essential factor regulating the molecule adsorption in vacuo, is balanced by the interaction of water molecules with both the adsorbate and the substrate. Consequently, the adsorption process is driven by the entropic contribution to the free energy, which favors the adsorption of the bases and the desorption of water molecules. Our results reveal the presence of a free energy barrier at relatively small molecule–surface distance, due to the competition between water and DNA molecules for the interaction with gold.

GoldDNA-AMBER offers a computationally accessible way to study the adsorption of DNA bases on the Au(111) surface, in different geometries, both in vacuo and in solution, while accounting for the dynamic polarization of the gold atoms. Its extension to the simulation of DNA oligomers laying flat on gold is a stepping stone toward revealing the effect of an inorganic surface on the state of folding of the double helix.

#### ■ ASSOCIATED CONTENT

##### Supporting Information

Section 1: additional technical details that complement section 2 and should allow reproducibility. Section 2: Text on the description of the procedure that was followed to set the parameters of the GoldDNA-AMBER FF; Tables S1–S4; Figures S1–S3. Table S1: LJ parameters for Au interacting with DNA bases. Table S2: DFT and FF formation energies of the training set of base@Au(111) structures in vacuo. Table S3: LJ parameters for Au interaction with water, for different water models. Table S4: energetics of water adsorption on Au(111) by DFT and FF calculations. Figure S1: training set of structures for the derivation of the GoldDNA-AMBER FF. Figure S2: correlation between vdW-DF and FF computed formation energies for the training set. Figure S3: adsorption structures for water on Au(111). Section 3: additional data on the energetics of periodic adsorbed adenine and guanine monolayers, reported in Tables S5 and S6. This material is available free of charge via the Internet at <http://pubs.acs.org/>.

#### ■ AUTHOR INFORMATION

##### Corresponding Author

\*E-mail: [rosa.difelice@unimore.it](mailto:rosa.difelice@unimore.it).

##### Notes

The authors declare no competing financial interest.

#### ■ ACKNOWLEDGMENTS

This work was funded by the Italian Institute of Technology through project MOPROSURF and the Computational Platform, by Fondazione Cassa di Risparmio di Modena through Progetto Internazionalizzazione 2011. The ISCR staff at CINECA (Bologna, Italy) is acknowledged for computational facilities and technical support.

#### ■ REFERENCES

- (1) Dovichi, N. J.; Zhang, J. *Angew. Chem., Int. Ed.* **2000**, 39, 4463–4468.
- (2) Porath, D.; Bezryadin, A.; de Vries, S.; Dekker, C. *Nature* **2000**, 403, 635–638.



- (3) Cohen, H.; Nogues, C.; Naaman, R.; Porath. *Proc. Natl. Acad. Sci. U.S.A.* **2005**, *102*, 11589–11593.
- (4) Xu, B.; Zhang, P.; Li, X.; Tao, N. *Nano Lett.* **2004**, *4*, 1105–1108.
- (5) Kang, N.; Erbe, A.; Scheer, E. *New J. Phys.* **2008**, *10*, 023030/1–9.
- (6) Boon, E. M.; Ceres, D. M.; Drummond, T. G.; Hill, M. G.; Barton, J. K. *Nat. Biotechnol.* **2000**, *18*, 1096–1100.
- (7) Zwolak, M.; Di Ventra, M. *Rev. Mod. Phys.* **2008**, *80*, 141–165.
- (8) He, H.; Scheicher, R. H.; Pandey, R.; Rocha, A. R.; Sanvito, S.; Grigoriev, A.; Ahuja, R. *J. Phys. Chem. C* **2008**, *112*, 3456–3459.
- (9) Shapir, E.; Cohen, H.; Calzolari, A.; Cavazzoni, C.; Ryndyk, D.; Cuniberti, G.; Kotlyar, A. B.; Di Felice, R.; Porath, D. *Nat. Mater.* **2008**, *7*, 68–74.
- (10) Shapir, E.; Sagiv, L.; Molotsky, T.; Kotlyar, A. B.; Di Felice, R.; Porath, D. *J. Phys. Chem. C* **2010**, *114*, 22079–22084.
- (11) de Pablo, P.; Moreno-Herrero, F.; Colchero, J.; Gomez-Herrero, J.; Herrero, P.; Baró, A. M.; Ordejón, P.; Soler, J. M.; Artacho, E. *Phys. Rev. Lett.* **2000**, *85*, 4992–4995.
- (12) Porath, D.; Cuniberti, G.; Di Felice, R. *Top. Curr. Chem.* **2004**, *237*, 183–227.
- (13) Endres, R. G.; Cox, D. L.; Singh, R. R. P. *Rev. Mod. Phys.* **2004**, *76*, 195–214.
- (14) Mallajosyula, S. S.; Pati, S. K. *J. Phys. Chem. Lett.* **2010**, *1*, 1881–1894.
- (15) Genereux, J. G.; Barton, J. K. *Chem. Rev.* **2010**, *110*, 1642–1662.
- (16) Kotlyar, A. B.; Borovok, N.; Molotsky, T.; Cohen, H.; Shapir, E.; Porath, D. *Adv. Mater.* **2005**, *17*, 1901–1905.
- (17) Varsano, D.; Garbesi, A.; Di Felice, R. *J. Phys. Chem. B* **2007**, *111*, 14012–14021.
- (18) Migliore, A.; Corni, S.; Varsano, D.; Klein, M. L.; Di Felice, R. *J. Phys. Chem. B* **2009**, *113*, 9402–9415.
- (19) Woiczikowski, P.; Kubar, T.; Gutierrez, R.; Caetano, R.; Cuniberti, G.; Elstner, M. *J. Chem. Phys.* **2009**, *130*, 215104/1–14.
- (20) Woiczikowski, P.; Kubar, T.; Gutierrez, R.; Cuniberti, G.; Elstner, M. *J. Chem. Phys.* **2010**, *133*, 035103/1–13.
- (21) Grozema, F. C.; Tonzani, S.; Berlin, Y. A.; Schatz, G. C.; Siebbeles, L. D. A.; Ratner, M. A. *J. Am. Chem. Soc.* **2008**, *130*, 5157–5166.
- (22) Patwardhan, S.; Tonzani, S.; Lewis, F. D.; Siebbeles, L. D. A.; Schatz, G. C.; Grozema, F. C. *J. Phys. Chem. B* **2012**, *116*, 11447–11458.
- (23) Daggett, V.; Levitt, M. *J. Mol. Biol.* **1993**, *232*, 600–619.
- (24) Tirado-Rives, J.; Orozco, M.; Jorgensen, W. L. *Biochem.* **1997**, *36*, 7313–7329.
- (25) Toofanny, R. D.; Daggett, V. *WIREs Comput. Mol. Sci.* **2012**, *2*, 405–423.
- (26) Pérez, A.; Orozco, M. *Angew. Chem., Int. Ed.* **2010**, *49*, 4805–4808.
- (27) Lee, O.-S.; Schatz, G. C. *J. Phys. Chem. C* **2009**, *113*, 2316–2321.
- (28) Iori, F.; Corni, S. *J. Comput. Chem.* **2008**, *29*, 1656–1666.
- (29) Iori, F.; Di Felice, R.; Molinari, E.; Corni, S. *J. Comput. Chem.* **2009**, *30*, 1465–1476.
- (30) Wright, L. B.; Rodger, P. M.; Corni, S.; Walsh, T. J. *Chem. Theory Comput.* **2013**, *9*, 1616–1630.
- (31) Kelly, R. E. A.; Xu, W.; Lukas, M.; Otero, R.; Mura, M.; Lee, Y.-J.; Laegsgaard, E.; Stensgaard, I.; Kantorovich, L. N.; Besenbacher, F. *Small* **2008**, *4*, 1494–1500.
- (32) Xu, W.; Kelly, R. E. A.; Henkjan, G.; Laegsgaard, E.; Stensgaard, I.; Kantorovich, L. N.; Besenbacher, F. *Small* **2009**, *5*, 1952–1956.
- (33) Redhead, P. A. *Vacuum* **1962**, *12*, 267.
- (34) Heinz, H.; Vaia, R. A.; Farmer, B. L.; Naik, R. R. *J. Phys. Chem. C* **2008**, *112*, 17281–17290.
- (35) Dauber-Osguthorpe, P.; Roberts, V. A.; Osguthorpe, D. J.; Wolff, J.; Genest, M.; Hagler, A. T. *Proteins: Struct., Funct., Genet.* **1988**, *4*, 31–47.
- (36) Jorgensen, W. L.; Maxwell, D. S.; Tirado-Rives, J. *J. Am. Chem. Soc.* **1996**, *118*, 11225–11236.
- (37) Brooks, B. R.; Brooks, C. L., III; Mackerell, A. D.; Nilsson, L.; Petrella, R. J.; Roux, B.; Won, Y.; Archontis, G.; Bartels, C.; Boresch, S.; Caflisch, A.; Caves, L.; Cui, Q.; Dinner, A. R.; Feig, M.; Fischer, S.; Gao, J.; Hodoscek, M.; Im, W.; Kucsera, K.; Lazaridis, T.; Ma, J.; Ovchinnikov, V.; Paci, E.; Pastor, R. W.; Post, C. B.; Pu, J. Z.; Schaefer, M.; Tidor, B.; Venable, R. M.; Woodcock, H. L.; Wu, X.; Yang, W.; York, D. M.; Karplus, M. *J. Comput. Chem.* **2009**, *30*, 1545–1614.
- (38) Rapino, S.; Zerbetto, F. *Langmuir* **2005**, *21*, 2512–2518.
- (39) Sändig, N.; Zerbetto, F. *Chem. Commun.* **2010**, *46*, 667–676.
- (40) Piana, S.; Billic, A. *J. Phys. Chem. B* **2006**, *110*, 23467–23471.
- (41) Heinz, H.; Farmer, B. L.; Pandey, R. B.; Slocik, J. M.; Patnaik, S. S.; Pachter, R.; Naik, R. R. *J. Am. Chem. Soc.* **2009**, *131*, 9704–9714.
- (42) Heinz, H.; Jha, K. C.; Luettmer-Strathmann, J.; Farmer, B. L.; Naik, R. R. *J. R. Soc. Interface* **2011**, *8*, 220–232.
- (43) Yu, J.; Becker, M. L.; Carri, G. A. *Small* **2010**, *6*, 2242–2245.
- (44) Yu, J.; Becker, M. L.; Carri, G. A. *Langmuir* **2012**, *28*, 1408–1417.
- (45) Feng, J.; Slocik, J. M.; Sarikaya, M.; Naik, R. R.; Farmer, B. L.; Heinz, H. *Small* **2012**, *8*, 1049–1059.
- (46) Rosa, M.; Corni, S.; Di Felice, R. *J. Phys. Chem. C* **2012**, *116*, 21366–21373.
- (47) Rosa, M.; Corni, S.; Di Felice, R. *J. Chem. Theory Comput.* **2013**, *9*, 4552–4561.
- (48) Ercolessi, F.; Parinello, M.; Tosatti, E. *Philos. Mag. A* **1988**, *58*, 213–226.
- (49) Cornell, W. D.; Cieplak, P.; Bayly, C. I.; Gould, I. R.; Merz, K. M., Jr.; Ferguson, D. M.; Spellmeyer, D. C.; Fox, T.; Caldwell, J. W.; Kollman, P. A. *J. Am. Chem. Soc.* **1995**, *117*, 5179–5197.
- (50) Perez, A.; Marchan, I.; Svozil, D.; Sponer, J.; Cheatham, T. E.; Laughton, C. A.; Orozco, M. *Biophys. J.* **2007**, *92*, 3817–3829.
- (51) Peréz, A.; Luque, F. J.; Orozco, M. *Acc. Chem. Res.* **2012**, *45*, 196–205.
- (52) Sorin, E. J.; Pande, V. S. *Biophys. J.* **2005**, *88*, 2472–2493.
- (53) DePaul, A. J.; Thompson, E. J.; Patel, S. S.; Haldeman, K.; Sorin, E. J. *Nucleic Acids Res.* **2010**, *38*, 4856–4867.
- (54) Hornak, V.; Abel, R.; Okur, A.; Strockbine, B.; Roitberg, A.; Simmerling, C. *Proteins: Struct., Funct., Bioinf.* **2006**, *65*, 712–725.
- (55) Collier, G.; Vellore, N. A.; Yancey, J. A.; Stuart, S. J.; Latour, R. A. *Biointerphases* **2012**, *7*, 24/1–19.
- (56) Vellore, N. A.; Yancey, J. A.; Collier, G.; Latour, R. A. *Langmuir* **2010**, *26*, 7396–7404.
- (57) Schravendijk, P.; Van Der Vegt, N.; Delle Site, L.; Kremer, K. *ChemPhysChem* **2005**, *6*, 1866–1871.
- (58) Ghiringhelli, L. M.; Hess, B.; van der Vegt, N.; Delle Site, L. *J. Am. Chem. Soc.* **2008**, *130*, 13460–13464.
- (59) Carravetta, V.; Monti, S. *J. Phys. Chem. B* **2006**, *110*, 6160–6169.
- (60) Schneider, J.; Colombi Ciacchi, L. *J. Chem. Theory Comput.* **2011**, *7*, 473–484.
- (61) Barone, V.; Casarin, M.; Forrer, D.; Monti, S.; Prampolini, G. *J. Phys. Chem. C* **2011**, *115*, 18434–18444.
- (62) Mendonca, A. C. F.; Malfreyt, P.; Padua, A. A. H. *J. Chem. Theory Comput.* **2012**, *8*, 3348–3355.
- (63) Ren, P.; Ponder, J. W. *J. Phys. Chem. B* **2004**, *108*, 13427–13437.
- (64) Harten, U.; Lahee, A. M.; Toennies, J. P.; Woll, C. *Phys. Rev. Lett.* **1985**, *54*, 2619–2622.
- (65) Iori, F.; Corni, S.; Di Felice, R. *J. Phys. Chem. C* **2008**, *112*, 13540–13545.
- (66) Giannozzi, P.; Baroni, S.; Bonini, N.; Calandra, M.; Car, R.; Cavazzoni, C.; Ceresoli, D.; Chiarotti, G. L.; Cococcioni, M.; Dabo, I.; Dal Corso, A.; de Gironcoli, S.; Fabris, S.; Fratesi, G.; Gebauer, R.; Gerstmann, U.; Gougoussis, C.; Kokalj, A.; Lazzeri, M.; Martin-Samos, L.; Marzari, N.; Mauri, F.; Mazzarello, R.; Paolini, S.; Pasquarello, A.; Paulatto, L.; Sbraccia, C.; Scandolo, S.; Sclauzero, G.; Seitsonen, A. P.; Smogunov, A.; Umari, P.; Wentzcovitch, R. M. *J. Phys.: Condens. Matter* **2009**, *21*, 395502/1–19.
- (67) Dion, M.; Rydberg, H.; Schroder, E.; Langreth, D. C.; Lundqvist, B. I. *Phys. Rev. Lett.* **2004**, *92*, 246401/1–4.

- (68) Thonhauser, T.; Cooper, V. R.; Li, S.; Puzder, A.; Hyldgaard, P.; Langreth, D. C. *Phys. Rev. B* **2007**, *76*, 125112/1–11.
- (69) Cooper, V. R. *Phys. Rev. B* **2010**, *81*, 161104(R)/1–4.
- (70) Langreth, D. C.; Dion, M.; Rydberg, H.; Schroder, E.; Hyldgaard, P.; Lundqvist, B. I. *Int. J. Quantum Chem.* **2005**, *101*, 599–610.
- (71) Puzder, A.; Dion, M.; Langreth, D. C. *J. Chem. Phys.* **2006**, *124*, 164105/1–8.
- (72) Lee, K.; Murray, E. D.; Kong, L.; Lundqvist, B. I.; Langreth, D. C. *Phys. Rev. B* **2010**, *82*, 081101(R)/1–4.
- (73) Rosa, M.; Corni, S.; Di Felice, R. Van der Waals effects in molecule–metal adsorption. Manuscript in preparation 2014.
- (74) Vanderbilt, D. *Phys. Rev. B* **1990**, *41*, R7892–R7895.
- (75) (a) Hess, B.; Kutzner, C.; van der Spoel, D.; Lindahl, E. *J. Chem. Theo. Comput.* **2008**, *4*, 435–447. (b) van der Spoel, D.; Lindahl, E.; Hess, B.; Groenhof, A. E. M.; Berendsen, H. J. C. *J. Comput. Chem.* **2005**, *26*, 1701–1718.
- (76) (a) Essman, U.; Perera, L.; Berkowitz, M. L.; Darden, T.; Lee, H.; Pedersen, L. G. *J. Chem. Phys.* **1995**, *103*, 8577–8592.
- (77) Lukas, M.; Kelly, R. E. A.; Kantorovich, L. N.; Otero, R.; Xu, W.; Laegsgaard, E.; Stensgaard, I.; Kantorovich, L. N.; Besenbacher, F. *J. Chem. Phys.* **2009**, *130*, 024705/1–9.
- (78) Xu, W.; Kelly, R. E. A.; Otero, R.; Schöck, M.; Laegsgaard, E.; Stensgaard, I.; Kantorovich, L. N.; Besenbacher, F. *Small* **2007**, *3*, 2011–2014.
- (79) Otero, R.; Lukas, W. X. M.; Kelly, R. E. A.; Xu, W.; Laegsgaard, E.; Stensgaard, I.; Kantorovich, L. N.; Besenbacher, F. *Science* **2008**, *319*, 312–315.
- (80) Kelly, R. E. A.; Lukas, M.; Kantorovich, L. N.; Otero, R.; Xu, W.; Mura, M.; Laegsgaard, E.; Stensgaard, I.; Besenbacher, F. *J. Chem. Phys.* **2008**, *129*, 187707/1–13.
- (81) Ostblom, M.; Liedberg, B.; Demers, L. M.; Mirkin, C. A. *J. Phys. Chem. B* **2005**, *109*, 15150–15160.
- (82) Faber, C.; Attacalite, C.; Olevano, V.; Runge, E.; Blase, X. *Phys. Rev. B* **2011**, *83*, 115123/1–5.
- (83) Neaton, J. B.; Hybertsen, M. S.; Louie, S. G. *Phys. Rev. Lett.* **2006**, *97*, 216405/1–4.
- (84) Tait, S. L.; Dohnálek, Z.; Campbell, C. T.; Kay, B. D. *J. Chem. Phys.* **2005**, *122*, 164708/1–9.
- (85) Campbell, C. T.; Sellers, J. R. *J. Am. Chem. Soc.* **2012**, *134*, 18109–18115.
- (86) Liu, W.; Ruiz, V. G.; Zhang, G. X.; Santral, B.; Ren, X.; Scheffler, M.; Tkatchenko, A. *New J. Phys.* **2013**, *15*, 053046/1–27.
- (87) Fichtorn, K. A.; Miron, R. A. *Phys. Rev. Lett.* **2002**, *89*, 196103/1–4.
- (88) Hess, B. *J. Chem. Phys.* **2002**, *116*, 209–217.